Differentiating contributions of electrons and phonons to the thermoreflectance spectra of gold

Kexin Liu,[1] Xinping Shi,[1] Frank Angeles,[1] Ramya Mohan,[2] Jon Gorchon,[3] Sinisa Coh,[1,2,*] and Richard B. Wilson[1,2,†]

[1]*Mechanical Engineering, University of California, Riverside, California 92521, USA*

[2]*Materials Science and Engineering, University of California, Riverside, California 92521, USA*

[3]*Université de Lorraine, CNRS, IJL, F-54000 Nancy, France*

(Received 4 February 2021; revised 10 September 2021; accepted 21 September 2021; published 22 October 2021)

To better understand the many effects of temperature on the optical properties of metals, we experimentally and theoretically quantify the electron vs phonon contributions to the thermoreflectance spectra of gold. We perform a series of pump/probe measurements on nanoscale Pt/Au bilayers at wavelengths between 400 and 1000 nm. At all wavelengths, we find that changes in phonon temperature, not electron temperature, are the primary contributor to the thermoreflectance of Au. The thermoreflectance is most sensitive to the electron temperature at a wavelength of ∼480 nm due to interband transitions between d states and the Fermi level. At 480 nm, the electron temperature is responsible for ∼20% of the total thermoreflectance. In the near infrared, the electron temperature is responsible for $< 2\%$ of the total thermoreflectance. We also compute the thermoreflectance spectra of Au from first principles. Our calculations further confirm that phonon temperature dominates thermoreflectance of Au. Most of the thermoreflectance of Au is due to the effect of the phonon population on electron lifetime.

DOI: 10.1103/PhysRevMaterials.5.106001

I. INTRODUCTION

Despite a half-century of study [1–15], the relative contributions of electrons vs phonons to the temperature dependence of the optical properties of a metal are not clear. A relatively common explanation for thermo-optic spectra of metals is that the electron temperature affects interband optical transitions [16–19]. An interband transition threshold is the energy difference between band extrema and the Fermi level. Absorption probabilities are higher for photon energies near the transition threshold. Therefore, a change in the electronic occupancy near the Fermi level can increase/decrease absorption for photons $k_B T$ above/below the interband transition threshold. This electron-temperature-based explanation for the thermoreflectance spectra is often invoked to explain the thermoreflectance spectra of simple metals Cu, Ag, and Au [19,20]. These metals have a maximum in their thermo-optic spectra near their interband transition thresholds. Other ways for the electron temperature to affect optical properties include altering electron-electron scattering rates [21] and shifting the Fermi level [1].

An alternative explanation for thermo-optic spectra of metals is thermal expansion [5]. Like changes in the electron occupancy, thermal expansion can also change the optical transition probabilities between band extrema and the Fermi level [5]. Since thermal expansion occurs because of increasing phonon populations, this explanation credits thermo-optic spectra to phonons. Additionally, electron-phonon interactions can affect optical properties [9,14]. Electron-phonon scattering rates are determined by the phonon temperature.

Experimentally evaluating the relative importance of electrons vs phonons to the thermo-optic spectra of metals is challenging. While many experimental studies report the thermoreflectance spectra of metals [1–15], these experiments were carried out at conditions where electrons and phonons were in equilibrium. To differentiate electron and phonon contributions to thermo-optic properties, the metal needs to be driven into a nonequilibrium state where electron and phonon temperatures differ $T_e \neq T_p$. Additionally, the nonequilibrium state needs to be such that the electron and phonon temperatures are definable. In other words, the electron distribution needs to be a Fermi-Dirac distribution, and the phonon distribution needs to be a Bose-Einstein distribution.

A straightforward way to cause nonequilibrium between electrons and phonons is photoexcitation [22]. However, photoexcitation drives the metal into a nonequilibrium state where the electrons and/or phonons have nonthermal distributions [18,23–26]. The distributions remain nonthermal until enough electron-electron, electron-phonon, and phonon-phonon scattering events occur to maximize entropy. Depending on the scattering rates, it takes between 0.1 and 5 ps for a nonthermal distribution to evolve into a thermal one [17,24,27]. This timescale is typically comparable with how long it takes for electrons and phonons to thermalize with each other [24]. In short, after photoexcitation, the electron and phonon temperatures may not be well defined until $T_e \approx T_p$. Several recent studies report that the nonthermal character of photoexcited electron distributions affects the optical response of metals in pump/probe experiments [17,18].

To overcome the challenge of nonthermal effects, we performed pump/probe measurements on Au/Pt bilayers. After

*sinisa.coh@gmail.com

†rwilson@ucr.edu

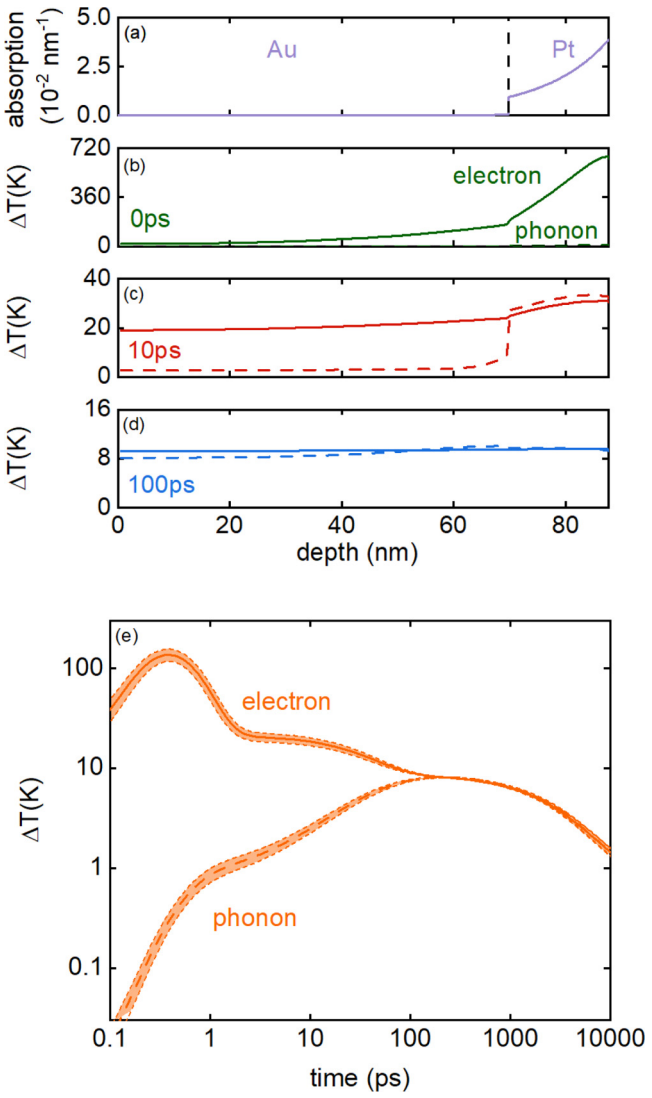

FIG. 1. Two temperature model calculations for the Au/Pt bilayer for a pump wavelength of 783 nm. (a) Absorption of the pump beam vs depth. (b)–(d) Electron temperature (solid lines) and phonon temperature (dashed lines) vs depth at delay times of 0, 10, and 100 ps. Nonequilibrium between electrons and phonons in the Au layer persists for ∼100 ps. (e) Electron and phonon temperature of the Au surface as a function of delay time. The shaded region represents the uncertainty in the electron and phonon temperature profiles due to uncertainties in thermal model parameters.

photoexcitation of the Pt layer, the electron and phonon temperatures in the Au are both definable and unequal on timescales between 2 and 100 ps after photoexcitation [28]. Unlike a single Au layer, where electrons and phonons take only a few picoseconds to thermalize after photoexcitation [17], electrons and phonons in a Au/Pt bilayer take as long as 100 ps to equilibrate [28,29]. We show the temperature dynamics after photoexcitation for a Au/Pt bilayer in Fig. 1. In a single Au film, the electron-phonon thermalization time is short because Au electrons have a small heat capacity. Alternatively, in a Au/Pt bilayer, the Au electrons, Pt electrons, and Pt phonons have strong enough thermal coupling to effectively form a single thermal reservoir [28,29]. Collectively, this reservoir has a heat capacity two orders of magnitude larger than Au electrons in isolation and therefore takes ∼100 times longer to thermalize with Au phonons. Another advantage of Au/Pt bilayers is that strong electron-electron interactions in Pt reduce the importance of nonthermal effects to the dynamics at all timescales [24,30].

The main results of our study are wavelength-dependent pump/probe measurements of Au/Pt bilayers. Our wavelength-dependent experiments reveal that the thermoreflectance of Au is primarily driven by changes in phonon temperature. The thermoreflectance of Au is most sensitive to electrons at 480 nm, where dR/dT_e makes up ∼20% of the total thermoreflectance. Alternatively, in the near infrared, the electron temperature is responsible for $< 2\%$ of the total thermoreflectance.

We also computed the thermoreflectance spectra of Au from first principles. Accurately calculating the thermoreflectance is challenging because of the multitude of ways that temperature affects optical properties. Nevertheless, in agreement with our experimental data, our first-principles calculations find that the dominant contribution to thermoreflectance spectra is through phonons. The large thermoreflectance of Au near the interband transition threshold is dominated by the temperature dependence of the electron lifetime due to electron-phonon interactions. Increases in the electron-phonon scattering rate decrease/increase absorption at wavelengths shorter/longer than the interband transition threshold wavelength of 510 nm.

II. EXPERIMENTAL METHODS

We deposited a 60 nm Au thin film and two Au/Pt bilayers on sapphire substrates for pump/probe experiments using a direct current magnetron sputter deposition system. The two bilayer samples are the focus of our study. The geometry of the two bilayer samples was (71 nm Au)/(17 nm Pt)/sapphire and (64 nm Au)/(19 nm Pt)/sapphire. Electron backscattering analyses show that the films are highly (111) textured. Further information on the sample preparation and our measurements of film thickness are provided in Ref. [31].

We performed front/back time-domain thermoreflectance measurements on the Pt/Au bilayers. By front/back, we mean the probe beam measures the Au reflectance at the front of the sample (Au/air interface), and the pump photoexcites the Pt layer through the back of the sample (Pt/sapphire interface). The pulse duration of the pump and probe beams was ∼100–200 fs. The pump beam was electro-optically modulated with a 50% duty cycle at 10.7 MHz. The intensity of the reflected probe pulse was monitored with an amplified silicon photodiode detector. The photodetector was connected to a radiofrequency lock-in that detected 10.7 MHz signal. Both pump and probe beams had a $1/e^2$ radius of ∼7 μm. We conducted experiments where the pump and probe beams had the same wavelength, tuned between 690 and 1000 nm. To extend the range of our study, we also conducted experiments with a frequency-doubled probe beam with wavelengths between 400 and 525 nm. Further details of our experimental setup are reported in Ref. [32].

We analyzed our pump/probe data with a two-temperature thermal model. The predictions of our thermal model for the

(71 nm Au)/(17 nm Pt) sample are summarized in Fig. 1. The model consists of two coupled heat equations for each layer in our sample. The heat equations describe how the electron and phonon temperatures evolve in space and time after photoexcitation with the pump:

$$C_e\frac{\partial T_e}{\partial t} = \Lambda_e\frac{\partial^2 T_e}{\partial z^2} + g_{\rm ep}(T_p - T_e) + S(z,t), \quad (1)$$

$$C_p\frac{\partial T_e}{\partial t} = \Lambda_p\frac{\partial^2 T_p}{\partial z^2} + g_{\rm ep}(T_e - T_p). \quad (2)$$

Here, T_e and T_p are the electron and phonon temperatures, C_e and C_p are the electron and phonon heat capacities, and $g_{\rm ep}$ is the electron-phonon energy transfer coefficient. The model considers where the heat is deposited via $S(z,t)$, which describes the absorption of optical energy by electrons (Fig. 1).

The input parameters of the thermal model are the thermal properties and optical constants of the sample. The outputs of the thermal model are the electron and phonon temperatures as a function of depth and time. All thermal model parameters we used to calculate the evolution of heat in the bilayer were fixed by independent measurements or literature values. To fix electronic thermal conductivities in our model, we sputtered separate 60- and 200-nm-thick Pt and Au single-layer films on sapphire. We then used the four-point probe method to measure the electrical resistivity of these films. Then using the Wiedemann-Franz law, we estimated $\Lambda_e \approx 190\,{\rm W\,m^{-1}\,K^{-1}}$ for Au and $\Lambda_e \approx 40\,{\rm W\,m^{-1}\,K^{-1}}$ for Pt. We assume that the electronic heat capacity scales linearly with electron temperature $C_e = \gamma T_e$. For Au, based on Ref. [29], we used $\gamma_{\rm Au} \approx 70\times10^{-6}\,{\rm J\,m^{-3}\,K^{-2}}$, $g_{\rm ep} \approx 2\times10^{16}\,{\rm W\,m^{-3}\,K^{-1}}$, $C_p \approx 2.5\,{\rm MJ\,m^{-3}\,K^{-1}}$, and $\Lambda_p \approx 3\,{\rm W\,m^{-1}\,K^{-1}}$. For Pt, based on Ref. [30], we used $\gamma_{\rm Pt} \approx 4\times10^{-4}\,{\rm J\,m^{-3}\,K^{-2}}$, $g_{\rm ep} \approx 6\times10^{17}\,{\rm W\,m^{-3}\,K^{-1}}$, $C_p \approx 2.7\,{\rm MJ\,m^{-3}\,K^{-1}}$, and $\Lambda_p \approx 7\,{\rm W\,m^{-1}\,K^{-1}}$. The shaded region in Fig. 2 indicates what range of electron and phonon temperatures is possible given uncertainties in the input parameters of the model.

We assume the time dependence of $S(z,t)$ tracks the intensity vs time of our laser pulse, which we previously measured and reported as a function of wavelength in Ref. [32]. Zero-delay time is defined as the time when the pump beam intensity is a maximum. This means that the pump pulse deposits half of its energy before zero-delay time. To determine the depth dependence of $S(z,t)$, we calculated the absorption profile using a multilayer reflectivity calculation like the one described in Ref. [29]. We used literature values for the indices of refraction of similarly prepared Au and Pt thin films [11]. The depth dependence of the absorption of the pump is shown in the top panel of Fig. 1 for a pump wavelength of 783 nm. In our experiments, as we changed the laser wavelength, the depth dependence of $S(z,t)$ was slightly altered due to the wavelength dependence of the index of refraction of Au and Pt. However, at all wavelengths that we conducted experiments, at least 97% of the energy of the pump pulse was absorbed directly by the Pt layer.

Solving Eqs. (1) and (2) requires boundary conditions. We couple phonon heat equations for Pt, Au, and sapphire by assuming the heat current carried by phonons across the interface is $J_p = G_{\rm int}\Delta T_p$, where ΔT_p is the phonon temperature difference across the interface, and $G_{\rm int}$ is the interfacial thermal conductance for either the Au/Pt or Pt/sapphire interface. We took $G_{\rm int}$ values from Ref. [29]. For boundary conditions on the electron heat equations, we assume an adiabatic boundary condition at the Pt/sapphire and Au/air interfaces. For electrons at the Au/Pt interface, the model assumes $J_e = G_{e-e}\Delta T_e$. Data for the electronic thermal conductance of Au/Pt interfaces is limited [29], but measurements of specific electrical resistance combined with the Wiedemann-Franz law [33] predict G_{e-e} of 10 and 30 $\rm GW\,m^{-2}\,K^{-1}$ for Pt/Cu and Pd/Au interfaces [34,35]. Our model predicts no detectable change in the temperature evolution of Au electrons and phonons for values of G_{e-e} ranging between 5 $\rm GW\,m^{-2}\,K^{-1}$ and infinity. Therefore, for simplicity, we set $G_{e-e} = \infty$, i.e., we assume the electron temperature is continuous across the Au/Pt interface.

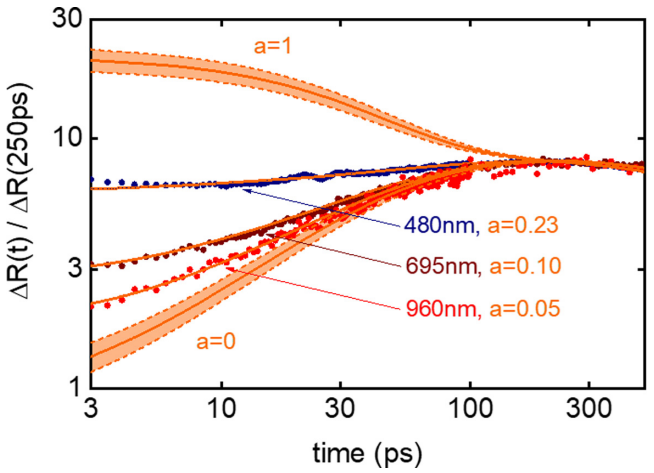

FIG. 2. Pump/probe data for the Au reflectance at 480, 695, and 960 nm. The transient reflectance of the Au layer depends on wavelength due to changes in electron vs phonon temperature sensitivity. Lines are thermal model predictions for the change in reflectance with different values for the electron temperature sensitivity parameter a. The shaded region represents our estimates for uncertainty in the electron and phonon temperature profiles due to uncertainties in thermal model parameters.

Our model predicts that heat is transported into the Au phonons in two ways. First, heat is exchanged between Au electrons and phonons due to the $g_{\rm ep}$ term in Eqs. (1) and (2). Second, heat can diffuse from the Pt phonons into the Au phonons due to a conductive boundary condition on the heat current at the Au/Pt interface (see Ref. [31] for more details). To qualitatively gauge the relative importance of these two heat-transfer mechanisms, we estimated the thermal conductance for these two processes. The effective conductance per unit area between Au electrons and Au phonons is $g_{\rm ep}^{\rm Au}d_{\rm Au} \approx 1\,{\rm GW\,m^{-2}\,K^{-1}}$, where $d_{\rm Au}$ is the length scale over which Au electrons and phonons are different temperatures. For a thick metal layer, this nonequilibrium length scale is $\approx\sqrt{\Lambda_e/g_{\rm ep}}$, which is ~100 nm for Au [29]. In our samples, the nonequilibrium length scale $d_{\rm Au}$ is limited by the ~70 nm thickness of the Au film. In contrast to the large electron-phonon conductance, a typical value for the phonon-phonon conductance at an interface between two materials is only

between 0.1 to 0.3 $\mathrm{GW\,m^{-2}\,K^{-1}}$ [36,37]. Therefore, we conclude electron-phonon energy exchange is the primary mechanism by which Au phonons are heated.

To compare with our experimental data, we parameterize the change in reflectance as

$$\Delta R(t) = C_{\mathrm{TR}}(\lambda)[a(\lambda)\Delta T_e(t) + b(\lambda)\Delta T_p(t)]. \quad (3)$$

Here, t is the time delay between the pump and probe pulses, $\Delta T_e(t)$ is the transient electron temperature, $\Delta T_p(t)$ is the transient phonon temperature, and $C_{\mathrm{TR}}(\lambda)$ describes the dependence of the thermoreflectance spectra on wavelength λ. We define C_{TR} as the magnitude of the equilibrium thermoreflectance coefficient $C_{\mathrm{TR}}(\lambda) = |dR/dT|$ when $\Delta T_e = \Delta T_p$. The functions $a(\lambda)$ and $b(\lambda)$ define the sensitivity of the thermoreflectance to electrons vs phonons. The relationship between these sensitivity functions and the partial derivatives of the reflectance is $\partial R/dT_e = a(\lambda)C_{\mathrm{TR}}(\lambda)$ and $\partial R/\partial T_{\mathrm{ph}} = b(\lambda)C_{\mathrm{TR}}(\lambda)$. The value of $a(\lambda) + b(\lambda)$ must equal 1 or -1, depending on whether the thermoreflectance is positive or negative at that λ. The temperatures $\Delta T_e(t)$ and $\Delta T_p(t)$ are a weighted average of the electron and phonon temperature profile as a function of depth [29]. The weighted average is calculated using a multilayer reflectivity calculation [38] that we describe in Ref. [31].

We do not consider the temperature dependence of $C_{\mathrm{TR}}(\lambda)$. Prior studies suggested the thermoreflectance of Au is nearly constant across temperatures between 300 and 500 K [15]. The temperature rise of the Au electrons in our experiment is < 200 K on timescales < 3 ps and < 20 K on the 3–200 ps timescales we fit our data across.

III. THEORETICAL METHODS

We used the first-principles calculated electron band structure energies $E_{n\mathbf{k}}$ and orbitals $\psi_{n\mathbf{k}}$ within the perturbative approach to evaluate the optical conductivity of Au [39,40]:

$$\sigma_{\alpha\beta}(\omega) = \frac{ie^2\hbar}{(2\pi)^3}\lim_{\mathbf{q}\to 0}\int dk \times \sum_{n,\,m}\frac{f_{m\mathbf{k}+\mathbf{q}} - f_{n\mathbf{k}}}{E_{m\mathbf{k}+\mathbf{q}} - E_{n\mathbf{k}}}\frac{\langle\psi_{n\mathbf{k}}v_\alpha\psi_{m\mathbf{k}+\mathbf{q}}\rangle\,\langle\psi_{m\mathbf{k}+\mathbf{q}}v_\beta\psi_{n\mathbf{k}}\rangle}{E_{m\mathbf{k}+\mathbf{q}} - E_{n\mathbf{k}} - \hbar\omega - i\eta_{mn\mathbf{k}}/2}. \quad (4)$$

The conductivity $\sigma_{\alpha\beta}$ describes the current in direction α in response to an electric field pointing in direction β. Equation (4) is a summation over possible electronic transitions between states in band m at wave vector $\mathbf{k}+\mathbf{q}$ to states in band n and wave vector $\mathbf{k}$. The limit as $\mathbf{q}\to 0$ indicates that we include both intraband and interband contributions to the optical conductivity. The Fermi-Dirac distribution occupation factor is denoted as f, while the velocity operator is denoted by v. Here, $\eta_{mn\mathbf{k}}$ describes the effect of electronic scattering rates on transitions due to electron-electron scattering. We treat the electron-phonon scattering via the special displacement method described in Ref. [41].

Electron and phonon temperatures appear at several places in the expression above for the optical conductivity. For example, the electron temperature T_e appears in the occupation factors $f_{n\mathbf{k}} \to f_{n\mathbf{k}}(T_e)$. However, the electron temperature also affects optical properties by altering electron-electron scattering rates $\eta_{mn\mathbf{k}} \to \eta_{mn\mathbf{k}}(T_e)$. Changes in phonon population alter $\psi_{n\mathbf{k}}$ and $E_{n\mathbf{k}}$ because electron-phonon interactions shift and warp energy bands (see Fig. 3). The phonon population also changes optical properties by modifying electron-phonon scattering rates. Finally, the phonon temperature T_p also affects Eq. (4) through the effect of volume expansion $V(T_p)$ on $\psi_{n\mathbf{k}}$ and $E_{n\mathbf{k}}$.

We treat the effect of phonon temperature on optical properties with the special displacement method approach described in Refs. [41,42]. In this approach, Au atoms in a supercell are displaced by vector ξ away from their equilibrium locations based on the phonon temperature T_p. As described in Ref. [41], vector ξ is computed as a sum over phonon eigenvectors, weighted by the Bose-Einstein occupation factor. Once we obtain the band structure for a system with displaced atoms, we recompute its optical conductivity. The special displacement method approach includes both Debye-Waller and Fan-Migdal electron-phonon terms and accurately describes the effects of electron-phonon interactions on both the real and imaginary part of the interband and intraband optical conductivity. The inclusion of both Debye-Waller and Fan-Migdal terms is an advantage over conventional treatments of electron-phonon interactions [14,43]. Similarly, we treat the effect of phonon-driven thermal expansion by computing the band structure and optical conductivity with different volume unit cells $\psi_{n\mathbf{k}} \to \psi_{n\mathbf{k}}[V(T_p)]$ and $E_{n\mathbf{k}} \to E_{n\mathbf{k}}[V(T_p)]$.

We model the temperature dependence of the electron-electron interaction contribution to carrier scattering rates using the Fermi liquid approach [44]:

$$\eta_{mn\mathbf{k}} = 0.0082\ \mathrm{eV^{-1}} \times \left[\tfrac{1}{2}(E_{m\mathbf{k}} - E_{\mathrm{F}})^2 + \tfrac{1}{2}(E_{n\mathbf{k}} - E_{\mathrm{F}})^2 + (\pi k_{\mathrm{B}}T_e)^2\right], \quad (5)$$

where we average the contribution of electron and hole state. We arrived at a prefactor of 0.0082 $\mathrm{eV^{-1}}$ by fitting to the first-principles GW calculations [45–47]. This prefactor is also consistent with two-photon photoemission data [48–50]. Importantly, Eq. (5) does not explicitly include the effects of electron-phonon interactions. Those effects are already included in our previously mentioned special displacement method approach.

Using the framework described above, we computed the thermoreflectance due to electron (T_e) or phonon (T_p) temperature with a finite-difference approach. Electron wave functions and energies were computed within the PBEsol + U approach as implemented in the QUANTUM ESPRESSO package [51]. We used $U = 2.7$ eV following Ref. [43]. We sampled the indirect absorption on a supercell containing 64 gold atoms. We sampled the charge density on a 24 × 24 × 24 mesh of k-points in the equivalent one-atom unit cell. The interband contributions to the optical conductivity were well converged with a 200 × 200 × 200 mesh of k-points in the equivalent one-atom unit cell. The intraband contributions converged at 40 × 40 × 40 mesh.

IV. RESULTS AND DISCUSSION

The change in reflectance of the Au layer after pump heating of the adjacent Pt layer is shown in Fig. 2 for probe

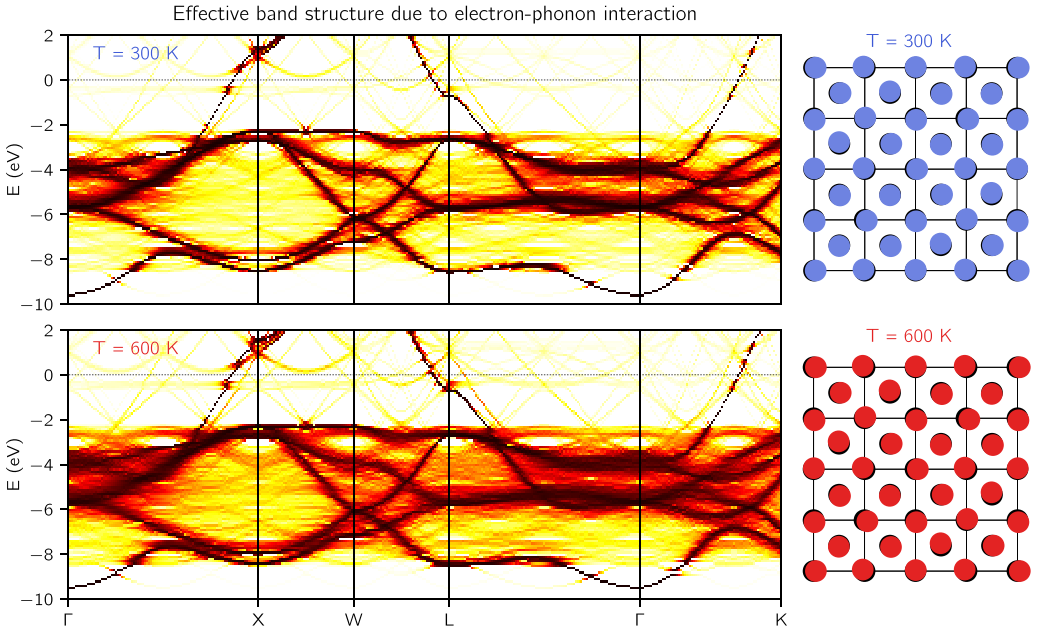

FIG. 3. Band structure of gold, including electron-phonon interaction contribution, along high-symmetry path in the Brillouin zone for temperature of 300 K (top) and 600 K (bottom). Calculations are done in a 4 × 4 × 4 supercell with thermal displacements of atoms (blue and red circles in the right panels). The band structure is unfolded into a primitive unit cell, as indicated with color on the plot. Darker colors correspond to larger intensity.

wavelengths of 480, 695, and 960 nm. For wavelengths in the near infrared, ΔR slowly increases for ∼100 ps after excitation. Alternatively, for wavelengths near the interband transition threshold of Au, e.g., 480 nm, ΔR depends only weakly on time after the first few picoseconds. We credit these differences in thermoreflectance signals at timescales between 2 and 100 ps to differences in sensitivity to the electron vs phonon temperatures.

We fit the data with Eq. (3) by treating the electron and phonon sensitivity parameters a and b as fit parameters at each wavelength, see Fig. 2. Figure 4 summarizes the best-fit values for $a(\lambda)$ at wavelengths between 400 and 1000 nm. The markers are the average value of $a(\lambda)$ we deduced by fitting data from both Pt/Au bilayer samples. The error bars account for the uncertainties in $\Delta T_p(t)$ and $\Delta T_e(t)$ due to uncertainties in the thermal model input parameters. Most of the uncertainty in $a(\lambda)$ arises from a 10% uncertainty in the thickness of the Pt film.

To test our concerns that nonthermal effects [17,18,24] prevent us from differentiating the effect of T_e vs T_p on thermoreflectance in a single Au layer, we also performed measurements on a 60 nm Au film with no Pt film. We used the values for $a(\lambda)$ shown in Fig. 4 to make two-temperature model predictions for $\Delta R(t)$ of the Au film. At some wavelengths, predictions for $\Delta R(t < 2\text{ps})$ disagree with the data in both magnitude and sign, see Ref. [31].

The values for $a(\lambda)$ and $b(\lambda)$ we derived from our experiments are intrinsic properties to Au and do not depend on the details of our sample geometry. The reflectance of the probe beam depends primarily on the optical properties of the Au

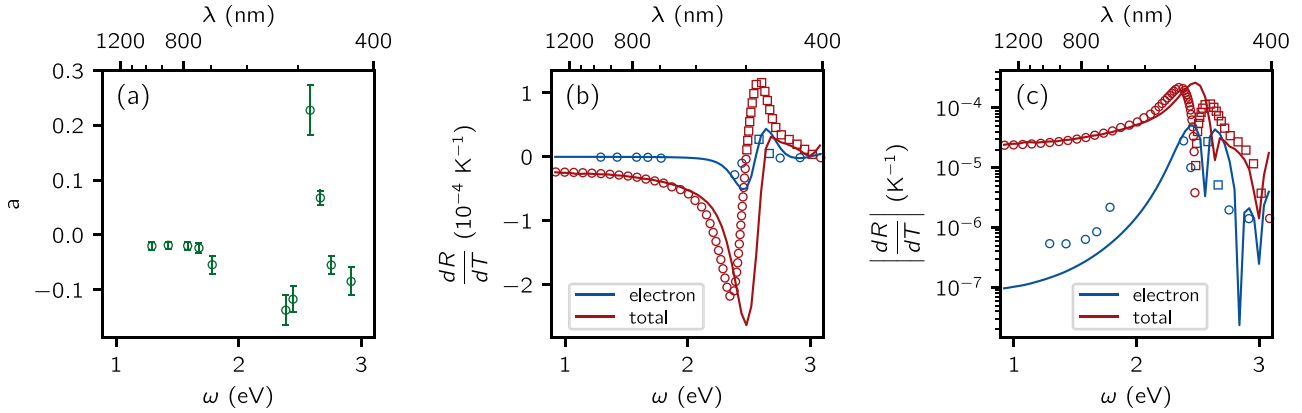

FIG. 4. (a) Sensitivity of the thermoreflectance to the electron temperature as a function of photon energy, $a(\omega)$. (b) and (c) Electron (blue) and total (red) thermoreflectance as a function of photon energy. Measured data are shown with symbols, while first-principles calculated results are shown with lines.

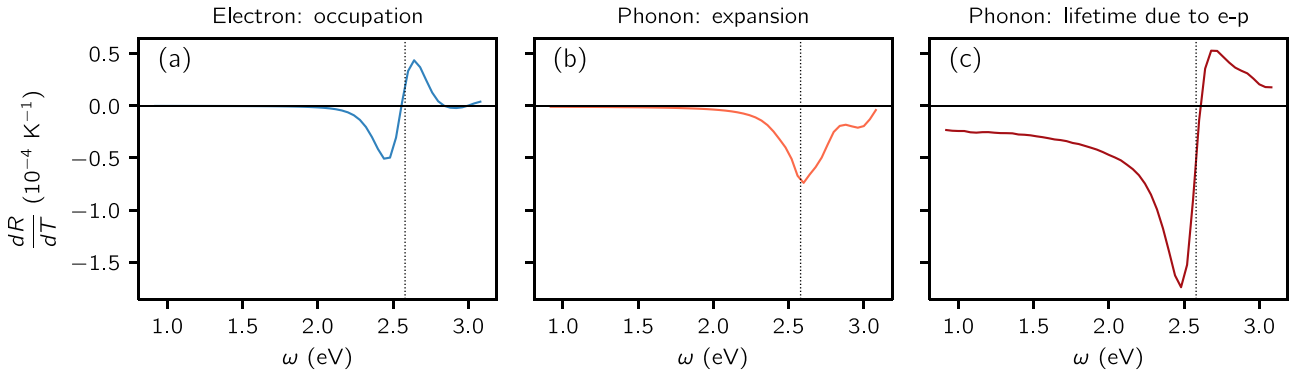

FIG. 5. Decomposition of the calculated thermoreflectance as a function of photon energy. Three panels show (a) contributions from the electron occupation, (b) volume expansion, and (c) thermally displaced atoms. The primary effect of thermally displaced atoms is on the electron-phonon lifetime.

layer because the Au thickness is much greater than the optical penetration depth. The optical penetration depth of Au is 16 and 12 nm for wavelengths of 400 and 1000 nm, respectively. However, there are uncertainties in the derived values of $a(\lambda)$ and $b(\lambda)$ due to the accuracy of thermal model predictions for the temperature evolution of the Au on timescales from 3 to 250 ps. To test the robustness of our thermal model predictions, we performed an additional experiment at 783 nm on a 73 nm Au/17 nm Fe sample. Like Pt, Fe has a much stronger electron-phonon energy transfer coefficient then Au. A best-fit value to our experimental data with our thermal model predictions for the Au/Fe yields $b(783\,\text{nm}) \approx 0.99$, see Ref. [31]. This value is in fair agreement with the value of $b(783\,\text{nm}) \approx -0.98 \pm 0.007$ we derived from the experiments on the two Au/Pt samples and supports our conclusion that phonons dominate the thermoreflectance spectra.

The results of our first-principles calculated thermoreflectance of Au are reported in Figs. 4 and 5. Overall, we find good quantitative and qualitative agreement with the experiment, as can be seen from Figs. 4(b) and 4(c). Our theory predicts that the total thermoreflectance of gold has a peak value of $-2.5 \times 10^{-4}\text{K}^{-1}$, in excellent agreement with experimental studies that report a peak thermoreflectance for Au between -2×10^{-4} and $-3 \times 10^{-4}\text{K}^{-1}$ [11,15,52]. We experimentally observe a maximum thermoreflectance at ∼540 nm, while theory predicts a maximum ∼520 nm. The theoretical predictions deviate from the experimental data at wavelengths < 520 nm, which is the interband transition threshold energy. There are two likely reasons for the discrepancy between experiment and theory at higher energies. First, the density functional theory is a ground-state theory. A fully rigorous description of optical properties requires a first-principles theory for the excited state, such as the GW-BSE approach. We do not use GW-BSE because its computational cost would make parts of our calculation infeasible, e.g., the special displacement method supercell approach for T_p effects. A second reason for discrepancy at high energy is the different elastic boundary condition in the model vs experiment. In our model, the bulk gold is free to expand in all directions. In the experiment, the gold film is deposited on a substrate that will hinder expansion in the directions parallel to the substrate.

Theory and experiment are also in agreement on how much the electron temperature affects the reflectance of Au, see Fig. 4(b). Theory predicts a maximum value of $|\partial R/\partial T_e| \approx 0.5 \times 10^{-4}\,\text{K}^{-1}$ for energies above and below the interband transition threshold. To deduce $|\partial R/\partial T_e|$ from our experimental measurements, we multiply $a(\lambda)$ reported in Fig. 4(a) with $C_{\text{TR}}(\lambda)$ reported in Ref. [11]. We arrive at a maximum value of $|\partial R/\partial T_e| \approx 0.3 \times 10^{-4}\,\text{K}^{-1}$. Like our theory predictions, the experimental maximum occurs above and below the interband transition threshold energy.

At longer wavelengths > 600 nm, the contribution of electrons to the total thermoreflectance is even less important. The total thermoreflectance in this energy range is $\sim -0.3 \times 10^{-4}\,\text{K}^{-1}$ in both theory and experiment. The electronic contribution is $\approx -5 \times 10^{-7}\,\text{K}^{-1}$ in experiment and between -10^{-6} and $-10^{-7}\,\text{K}^{-1}$ in our calculation. Therefore, we conclude that, at all energies, thermoreflectance of Au is dominated by the phonon temperature.

The primary way thermally displaced atoms $\xi(T_p)$ affect the dielectric function is through modifications in the electron-phonon lifetime. To confirm this, we did a new calculation with two differences from the approach described above. First, we removed the effect of thermally displaced atoms from our calculation. Second, we added an electron-phonon scattering term to electron lifetime in Eq. (5) that is proportional to T_p. We set the proportionality constant based on the temperature dependence of the electrical conductivity. We found this simple but crude method for including the effects of electron-phonon scattering qualitatively reproduces the thermoreflectance predicted by the special displacement method approach. Our findings in Fig. 5 correct older band structure studies that concluded thermoreflectance spectra were primarily due to thermal expansion [5,9].

V. CONCLUSIONS

We have experimentally determined that phonons dominate the thermoreflectance spectra of Au. By experimentally quantifying the sensitivity of the thermoreflectance spectra to electron vs phonon temperatures, it is now possible to use time-domain thermoreflectance experiments to differentiate between ultrafast electron vs phonon dynamics in metal films. Previously, such a differentiation had only been possible using time-resolved x-ray diffraction experiments [53]. Our first-principles calculations show that phonons dominate the

thermoreflectance spectra by changing the electron lifetime due to electron-phonon interactions. While this paper focuses only on Au, we expect our conclusions will be applicable to other metals for several reasons. Many metals, e.g., Al, Ta, Cu, and Ag, have sharp resonancelike features in the thermoreflectance spectra near interband transition threshold energies. These similarities in thermoreflectance spectra suggest similar origins. Furthermore, most metals have significantly stronger electron-phonon coupling than the heavy metal Au since the strength of electron-phonon interactions depends on atomic mass. Stronger electron-phonon interactions will increase the dependence of the dielectric function on phonon temperature.

Our findings are important for understanding and interpreting phenomena in many fields, including nanophotonics and plasmonics [54–56], ultrafast electron dynamics [16,17,57,58], ultrafast magnetism [59–63], and nanoscale heat transfer [64–66]. Scientists in these fields use optical pump/probe experiments to study charge and energy transport in plasmonic and nanophotonic devices [18,54–56] or nanoscale metal multilayers [28,30,59–63,67–69]. Important length scales in pump/probe measurements of metal structures and devices are <100 nm . Important time scales are <100 ps [28]. At these short length and time scales, electrons and phonons in the metal can be out of equilibrium [24,70,71]. Knowledge of how and why the optical properties of a metal depend on the phonon vs electron temperature will aid the interpretation of pump/probe measurements of nonequilibrium phenomena [17,54,65,68,70–72].

ACKNOWLEDGMENTS

We thank Ivo Souza for his assistance with the WANNIER90 code. The work by K.L., X.S., R.M., and R.W. was primarily supported by the U.S. Army Research Laboratory and the U.S. Army Research Office under Contract/Grant No. W911NF-18-1-0364. K.L. and R.W. also acknowledge support by the National Science Foundation (NSF; CBET—1847632). S.C. was supported by NSF (DMR-1848074). We also thank the French PIA project "Lorraine Université d'Excellence" reference ANR-15-IDEX-04-LUE. Work by J.G. was supported as part of the project PLUS by the Metropole Grand Nancy, the ANR project ANR-20-CE24-0003 and the "FEDER-FSE Lorraine et Massif Vosges 2014–2020," a European Union Program.

[1] R. Rosei and D. W. Lynch, Thermomodulation spectra of Al, Au, and Cu, Phys. Rev. B **5**, 3883 (1972).

[2] R. Rosei, F. Antonangeli, and U. Grassano, *d* bands position and width in gold from very low temperature thermomodulation measurements, Surf. Sci. **37**, 689 (1973).

[3] R. Rosei, C. Culp, and J. Weaver, Temperature modulation of the optical transitions involving the Fermi surface in Ag: experimental, Phys. Rev. B **10**, 484 (1974).

[4] E. Colavita, S. Modesti, and R. Rosei, Thermoreflectance of Ag single crystals, Phys. Rev. B **14**, 3415 (1976).

[5] P. Winsemius, F. Van Kampen, H. Lengkeek, and C. Van Went, Temperature dependence of the optical properties of Au, Ag and Cu, J. Phys. F Met. Phys. **6**, 1583 (1976).

[6] P. B. Johnson and R. W. Christy, Optical constants of copper and nickel as a function of temperature, Phys. Rev. B **11**, 1315 (1975).

[7] J. H. Weaver, C. G. Olson, D. W. Lynch, and M. Piancentini, Thermoreflectance of Mo from 0.5 to 35 eV, Solid State Commun. **16**, 163 (1975).

[8] W. Scouler, Temperature-Modulated Reflectance of Gold from 2 to 10 eV, Phys. Rev. Lett. **18**, 445 (1967).

[9] N. E. Christensen and B. O. Seraphin, Relativistic band calculation and the optical properties of gold, Phys. Rev. B **4**, 3321 (1971).

[10] C. A. Paddock and G. L. Eesley, Transient thermoreflectance from thin metal films, J. Appl. Phys. **60**, 285 (1986).

[11] R. Wilson, B. A. Apgar, L. W. Martin, and D. G. Cahill, Thermoreflectance of metal transducers for optical pump-probe studies of thermal properties, Opt. Express **20**, 28829 (2012).

[12] H. Reddy, U. Guler, A. V. Kildishev, A. Boltasseva, and V. M. Shalaev, Temperature-dependent optical properties of gold thin films, Opt. Mater. Express **6**, 2776 (2016).

[13] P.-T. Shen, Y. Sivan, C.-W. Lin, H.-L. Liu, C.-W. Chang, and S.-W. Chu, Temperature- and roughness-dependent permittivity of annealed/unannealed gold films, Opt. Express **24**, 19254 (2016).

[14] M. Xu, J.-Y. Yang, S. Zhang, and L. Liu, Role of electron-phonon coupling in finite-temperature dielectric functions of Au, Ag, and Cu, Phys. Rev. B **96**, 115154 (2017).

[15] T. Favaloro, J.-H. Bahk, and A. Shakouri, Characterization of the temperature dependence of the thermoreflectance coefficient for conductive thin films, Rev. Sci. Instrum. **86**, 024903 (2015).

[16] J. Hohlfeld, S.-S. Wellershoff, J. Güdde, U. Conrad, V. Jähnke, and E. Matthias, Electron and lattice dynamics following optical excitation of metals, Chem. Phys. **251**, 237 (2000).

[17] T. Heilpern, M. Manjare, A. O. Govorov, G. P. Wiederrecht, S. K. Gray, and H. Harutyunyan, Determination of hot carrier energy distributions from inversion of ultrafast pump-probe reflectivity measurements, Nat. Commun. **9**, 1853 (2018).

[18] A. M. Brown, R. Sundararaman, P. Narang, A. M. Schwartzberg, W. A. Goddard, and H. A. Atwater, Experimental and *Ab Initio* Ultrafast Carrier Dynamics in Plasmonic Nanoparticles, Phys. Rev. Lett. **118**, 087401 (2017).

[19] M. Dresselhaus, *Solid State Physics Part II Optical Properties of Solids*, Lecture Notes (Massachusetts Institute of Technology, Cambridge, 2001), Vol. 17, pp. 15–16.

[20] K. H. Bennemann, *Non-Linear Optics in Metals* (Oxford University Press, Oxford, 1998).

[21] X. Wang, D. M. Riffe, Y.-S. Lee, and M. Downer, Time-resolved electron-temperature measurement in a highly excited gold target using femtosecond thermionic emission, Phys. Rev. B **50**, 8016 (1994).

[22] S. Brorson, A. Kazeroonian, J. Moodera, D. Face, T. Cheng, E. Ippen, M. Dresselhaus, and G. Dresselhaus, Femtosecond

Room-Temperature Measurement of the Electron-Phonon Coupling Constant γ in Metallic Superconductors, Phys. Rev. Lett. **64**, 2172 (1990).

[23] P. Maldonado, K. Carva, M. Flammer, and P. M. Oppeneer, Theory of out-of-equilibrium ultrafast relaxation dynamics in metals, Phys. Rev. B **96**, 174439 (2017).

[24] R. B. Wilson and S. Coh, Parametric dependence of hot electron relaxation timescales on electron-electron and electron-phonon interaction strengths, Commun. Phys. **3**, 179 (2020).

[25] L. Waldecker, R. Bertoni, R. Ernstorfer, and J. Vorberger, Electron-Phonon Coupling and Energy Flow in a Simple Metal beyond the Two-Temperature Approximation, Phys. Rev. X **6**, 021003 (2016).

[26] K. Sokolowski-Tinten, X. Shen, Q. Zheng, T. Chase, R. Coffee, M. Jerman, R. Li, M. Ligges, I. Makasyuk, and M. Mo, Electron-lattice energy relaxation in laser-excited thin-film Au-insulator heterostructures studied by ultrafast MeV electron diffraction, Struct. Dyn. **4**, 054501 (2017).

[27] T. Chase, M. Trigo, A. Reid, R. Li, T. Vecchione, X. Shen, S. Weathersby, R. Coffee, N. Hartmann, and D. Reis, Ultrafast electron diffraction from non-equilibrium phonons in femtosecond laser heated Au films, Appl. Phys. Lett. **108**, 041909 (2016).

[28] W. Wang and D. G. Cahill, Limits to Thermal Transport in Nanoscale Metal Bilayers due to Weak Electron-Phonon Coupling in Au and Cu, Phys. Rev. Lett. **109**, 175503 (2012).

[29] G.-M. Choi, R. B. Wilson, and D. G. Cahill, Indirect heating of Pt by short-pulse laser irradiation of Au in a nanoscale Pt/Au bilayer, Phys. Rev. B **89**, 064307 (2014).

[30] H. Jang, J. Kimling, and D. G. Cahill, Nonequilibrium heat transport in Pt and Ru probed by an ultrathin Co thermometer, Phys. Rev. B **101**, 064304 (2020).

[31] See Supplemental Material at http://link.aps.org/supplemental/10.1103/PhysRevMaterials.5.106001 for additional pump/probe data, details on sample characterization, and thermoreflectance modeling.

[32] M. J. Gomez, K. Liu, J. G. Lee, and R. B. Wilson, High sensitivity pump-probe measurements of magnetic, thermal, and acoustic phenomena with a spectrally tunable oscillator, Rev. Sci. Instrum. **91**, 023905 (2020).

[33] R. Wilson and D. G. Cahill, Experimental Validation of the Interfacial Form of the Wiedemann-Franz Law, Phys. Rev. Lett. **108**, 255901 (2012).

[34] H. Kurt, R. Loloee, K. Eid, W. Pratt Jr, and J. Bass, Spin-Memory Loss at 4.2 K in Sputtered Pd and Pt and at Pd/Cu and Pt/Cu Interfaces, Appl. Phys. Lett. **81**, 4787 (2002).

[35] C. Galinon, K. Tewolde, R. Loloee, W.-C. Chiang, S. Olson, H. Kurt, W. Pratt Jr, J. Bass, P. Xu, and K. Xia, Pd/Ag and Pd/Au interface specific resistances and interfacial spin flipping, Appl. Phys. Lett. **86**, 182502 (2005).

[36] R. Wilson, B. A. Apgar, W.-P. Hsieh, L. W. Martin, and D. G. Cahill, Thermal conductance of strongly bonded metal-oxide interfaces, Phys. Rev. B **91**, 115414 (2015).

[37] C. Monachon, L. Weber, and C. Dames, Thermal boundary conductance: A materials science perspective, Annu. Rev. Mater. Res. **46**, 433 (2016).

[38] E. Hecht, *Optics* (Addison Wesley, San Francisco, CA, 1998).

[39] S. L. Adler, Quantum theory of the dielectric constant in real solids, Phys. Rev. **126**, 413 (1962).

[40] N. Wiser, Dielectric constant with local field effects included, Phys. Rev. **129**, 62 (1963).

[41] M. Zacharias and F. Giustino, One-shot calculation of temperature-dependent optical spectra and phonon-induced band-gap renormalization, Phys. Rev. B **94**, 075125 (2016).

[42] M. Zacharias and F. Giustino, Theory of the special displacement method for electronic structure calculations at finite temperature, Phys. Rev. Research **2**, 013357 (2020).

[43] A. M. Brown, R. Sundararaman, P. Narang, W. A. Goddard, and H. A. Atwater, *Ab initio* phonon coupling and optical response of hot electrons in plasmonic metals, Phys. Rev. B **94**, 075120 (2016).

[44] J. Sólyom, *Fundamentals of the Physics of Solids: Volume 3—Normal, Broken-Symmetry, and Correlated Systems* (Springer-Verlag, Berlin, Heidelberg, 2010).

[45] I. Campillo, J. M. Pitarke, A. Rubio, and P. M. Echenique, Role of occupied *d* states in the relaxation of hot electrons in Au, Phys. Rev. B **62**, 1500 (2000).

[46] F. Ladstädter, U. Hohenester, P. Puschnig, and C. Ambrosch-Draxl, First-principles calculation of hot-electron scattering in metals, Phys. Rev. B **70**, 235125 (2004).

[47] M. Bernardi, J. Mustafa, J. B. Neaton, and S. G. Louie, Theory and computation of hot carriers generated by surface plasmon polaritons in noble metals, Nat. Commun. **6**, 7044 (2015).

[48] R. Bauer, A. Schmid, P. Pavone, and D. Strauch, Electron-phonon coupling in the metallic elements Al, Au, Na, and Nb: a first-principles study, Phys. Rev. B **57**, 11276 (1998).

[49] J. Cao, Y. Gao, H. E. Elsayed-Ali, R. J. D. Miller, and D. A. Mantell, Femtosecond photoemission study of ultrafast electron dynamics in single-crystal Au(111) films, Phys. Rev. B **58**, 10948 (1998).

[50] M. Aeschlimann, M. Bauer, S. Pawlik, R. Knorren, G. Bouzerar, and K. Bennemann, Transport and dynamics of optically excited electrons in metals, Appl. Phys. A **71**, 485 (2000).

[51] P. Giannozzi, O. Baseggio, P. Bonfà, D. Brunato, R. Car, I. Carnimeo, C. Cavazzoni, S. De Gironcoli, P. Delugas, and F. Ferrari Ruffino, QUANTUM ESPRESSO toward the exascale, J. Chem. Phys. **152**, 154105 (2020).

[52] M. Otter, Temperaturabhängigkeit der optischen konstanten massiver metalle, Z. Phys. **161**, 539 (1961).

[53] J. Pudell, A. Maznev, M. Herzog, M. Kronseder, C. Back, G. Malinowski, A. Von Reppert, and M. Bargheer, Layer specific observation of slow thermal equilibration in ultrathin metallic nanostructures by femtosecond x-ray diffraction, Nat. Commun. **9**, 3335 (2018).

[54] O. Lozan, R. Sundararaman, B. Ea-Kim, J.-M. Rampnoux, P. Narang, S. Dilhaire, and P. Lalanne, Increased rise time of electron temperature during adiabatic plasmon focusing, Nat. Commun. **8**, 1656 (2017).

[55] M.-N. Su, C. J. Ciccarino, S. Kumar, P. D. Dongare, S. A. Hosseini Jebeli, D. Renard, Y. Zhang, B. Ostovar, W.-S. Chang, P. Nordlander, N. J. Halas, R. Sundararaman, P. Narang, and S. Link, Ultrafast electron dynamics in single aluminum nanostructures, Nano Lett. **19**, 3091 (2019).

[56] G. Tagliabue, A. S. Jermyn, R. Sundararaman, A. J. Welch, J. S. DuChene, R. Pala, A. R. Davoyan, P. Narang, and H. A. Atwater, Quantifying the role of surface plasmon excitation and hot carrier transport in plasmonic devices, Nat. Commun. **9**, 3394 (2018).

[57] E. L. Radue, J. A. Tomko, A. Giri, J. L. Braun, X. Zhou, O. V. Prezhdo, E. L. Runnerstrom, J.-P. Maria, and P. E. Hopkins, Hot electron thermoreflectance coefficient of gold during electron-phonon nonequilibrium, ACS Photonics **5**, 4880 (2018).

[58] A. Block, M. Liebel, R. Yu, M. Spector, Y. Sivan, F. J. García de Abajo, and N. F. van Hulst, Tracking ultrafast hot-electron diffusion in space and time by ultrafast thermomodulation microscopy, Sci. Adv. **5**, eaav8965 (2019).

[59] R. B. Wilson, J. Gorchon, Y. Yang, C.-H. Lambert, S. Salahuddin, and J. Bokor, Ultrafast magnetic switching of GdFeCo with electronic heat currents, Phys. Rev. B **95**, 180409 (2017).

[60] G.-M. Choi, B.-C. Min, K.-J. Lee, and D. G. Cahill, Spin current generated by thermally driven ultrafast demagnetization, Nat. Commun. **5**, 4334 (2014).

[61] G.-M. Choi, C.-H. Moon, B.-C. Min, K.-J. Lee, and D. G. Cahill, Thermal spin-transfer torque driven by the spin-dependent Seebeck effect in metallic spin-valves, Nat. Phys. **11**, 576 (2015).

[62] J. Kimling, G.-M. Choi, J. T. Brangham, T. Matalla-Wagner, T. Huebner, T. Kuschel, F. Yang, and D. G. Cahill, Picosecond Spin Seebeck Effect, Phys. Rev. Lett. **118**, 057201 (2017).

[63] T. S. Seifert, S. Jaiswal, J. Barker, S. T. Weber, I. Razdolski, J. Cramer, O. Gueckstock, S. F. Maehrlein, L. Nadvornik, S. Watanabe, C. Ciccarelli, A. Melnikov, G. Jakob, M. Münzenberg, S. T. B. Goennenwein, G. Woltersdorf, B. Rethfeld, P. W. Brouwer, M. Wolf, M. Kläui *et al.*, Femtosecond formation dynamics of the spin Seebeck effect revealed by terahertz spectroscopy, Nat. Commun. **9**, 2899 (2018).

[64] K. T. Regner, L. C. Wei, and J. A. Malen, Interpretation of thermoreflectance measurements with a two-temperature model including non-surface heat deposition, J. Appl. Phys. **118**, 235101 (2015).

[65] R. Wilson, J. P. Feser, G. T. Hohensee, and D. G. Cahill, Two-channel model for nonequilibrium thermal transport in pump-probe experiments, Phys. Rev. B **88**, 144305 (2013).

[66] D. G. Cahill, P. V. Braun, G. Chen, D. R. Clarke, S. Fan, K. E. Goodson, P. Keblinski, W. P. King, G. D. Mahan, and A. Majumdar, Nanoscale thermal transport. II. 2003–2012, Appl. Phys. Rev. **1**, 011305 (2014).

[67] J. Kimling and D. G. Cahill, Spin diffusion induced by pulsed-laser heating and the role of spin heat accumulation, Phys. Rev. B **95**, 014402 (2017).

[68] J. Kimling, R. Wilson, K. Rott, J. Kimling, G. Reiss, and D. G. Cahill, Spin-dependent thermal transport perpendicular to the planes of Co/Cu multilayers, Phys. Rev. B **91**, 144405 (2015).

[69] J. Gorchon, R. B. Wilson, Y. Yang, A. Pattabi, J. Y. Chen, L. He, J. P. Wang, M. Li, and J. Bokor, Role of electron and phonon temperatures in the helicity-independent all-optical switching of GdFeCo, Phys. Rev. B **94**, 184406 (2016).

[70] A. A. Maznev, J. A. Johnson, and K. A. Nelson, Non-equilibrium transient thermal grating relaxation in metal, J. Appl. Phys. **109**, 073517 (2011).

[71] J. P. Freedman, R. F. Davis, and J. A. Malen, Nondiffusive electron transport in metals: a two-temperature Boltzmann transport equation analysis of thermoreflectance experiments, Phys. Rev. B **99**, 054308 (2019).

[72] Y. Sivan and M. Spector, Ultrafast dynamics of optically-induced heat gratings in metals—more complicated than expected, arXiv:1909.03122.